THE ASTROPHYSICAL JOURNAL, 311:595–609, 1986 December 15

SYNCHROTRON AND INVERSE COMPTON EMISSION FROM EXPANDING SOURCES IN JETS: APPLICATION TO SS 433

DAVID L. BAND
IGPP—Lawrence Livermore National Laboratory
AND
JONATHAN E. GRINDLAY
Harvard-Smithsonian Center for Astrophysics
Received 1985 October 21; accepted 1986 May 29

ABSTRACT

The formalism for an expanding source is extended to include continuous injection of electrons and the production of X-rays by both inverse Compton scattering of external photons and synchrotron-self-Compton scattering. The resulting model is applied to the expanding nonthermal sources entrained in the jets of SS 433. We find that these sources can produce both the flaring radio component and the X-ray fluxes only if the relativistic electrons and the magnetic field are far out of equipartition. If the expanding source in the jets is in equipartition, the X-rays may originate from a stationary source within the binary system which is self-absorbed at radio frequencies and produces X-rays by inverse Compton scattering of optical photons from the binary. The resulting model of SS 433 is similar to that of radio-quiet AGN discussed in Band and Grindlay.

Subject headings: galaxies: nuclei — quasars — radiation mechanisms — stars: binaries — stars: individual

I. INTRODUCTION

Recent observations of flaring events and expanding knots in galactic and extragalactic jets warrants a reexamination of the modeling of expanding sources entrained in jets. Knots in 3C 273 have been observed to separate from the core (Unwin *et al.* 1985; Marscher and Gear 1985), while within our Galaxy flares associated with expanding radio sources have been observed in SS 433 (see Spencer 1984 for a summary) and Cygnus X-3 (Johnston *et al.* 1985; Molnar, Reid, and Grindlay 1984, 1985; Molnar 1985). The wealth of data shows that simple models of an expanding source are insufficient to describe the observed source evolutions. In many sources, such as 3C 273 (Peterson and Dent 1976), SS 433 (Seaquist *et al.* 1982, hereafter SGJG), and Cygnus X-3 (Molnar 1985), additional electrons must be injected into the source as it expands. In addition, the observed correlation between the X-ray and radio flares of SS 433, which were modeled by SGJG as originating in the jets, suggests that X-ray production be added to these models. Consequently, we present a general model for expanding sources as they might appear entrained in a jet. We then explore the consequences of this model for the radio and X-ray emitting regions of SS 433.

The seminal paper of van der Laan (1966) presents the standard model of a source expanding spherically at a constant rate with an initial complement of electrons that cool adiabatically. Peterson and Dent (1976) included continuous electron injection in modeling radio flares from 3C 273. Marscher and Brown (1975) considered both the effects of free-free absorption within the source and the evolution of the electron distribution where both adiabatic and synchrotron losses are important. The evolution of the X-ray spectrum from an expanding source has yet to be considered.

The X-ray and radio observations of SS 433 permit detailed modeling of the source. SGJG explained two simultaneous X-ray and radio flares as synchrotron and inverse Compton scattering from expanding nonthermal sources (called "plasmons" by SGJG) entrained in the jets at a distance of $\sim 10^{15}$ cm from the binary system. Radio knots associated with these flares are observed to separate from the central source (Spencer 1984). Band and Grindlay (1984, hereafter BG84) attribute these events to accretion surges triggered by variations of the Roche geometry of the binary system. However, Grindlay *et al.* (1984, hereafter GB84) observed an apparent partial X-ray eclipse (the data are insufficient to determine whether the eclipse was total) at the orbital phase when the compact object is eclipsed in the standard binary model. This probable partial eclipse has been confirmed by *EXOSAT* (Watson *et al.* 1986). This would indicate that a substantial fraction of the X-rays are produced within the binary system and not in the radio-producing expanding source in the jets.

EXOSAT has also observed iron line emission with 0.5 keV equivalent width, indicating that a significant portion of the X-ray continuum must be thermal if the hot thermal gas has normal abundances (Watson *et al.* 1986). The iron line is Doppler-shifted to higher frequencies with a frequency shift consistent with emission within the blueshifted jet inferred from the "moving" optical lines. The redshifted X-ray line is not seen and may be hidden by the accretion disk, suggesting that the jet accelerates, and the thermal X-rays are emitted, within 10^{12} cm of the compact object (Watson *et al.* 1986). In contrast, the *Einstein* observations (GB84) are best fitted by a nonthermal power law with a time-varying spectral index, and no thermal limes were detected (although the *EXOSAT* detection is consistent with the 2 σ *Einstein* upper limit).

Thus the *Einstein* observations indicate nonthermal X-ray emission, while the *EXOSAT* observations show the presence of a thermal component. In addition, *EXOSAT* did not detect any X-ray flares, but did find a total flux substantially higher than that observed by *Einstein*. Radio flares were observed during the *Einstein* observations (SGJG), while *EXOSAT* observed SS 433 when the radio source was quiescent (Fiedler 1986, private communication). These differences in the radio and X-ray emissions between the *Einstein* and *EXOSAT* observations suggest that the source is characterized by two states: a flaring state with nonthermal X-ray

emission, and a quiescent state with more luminous, partially thermal X-ray emission. The relative proportions of thermal and nonthermal emission in each of these states is as yet unclear. Nevertheless, we will assume throughout that during the *Einstein* observations the X-ray emissions from SS 433 are nonthermal, with the *EXOSAT* results confirming that at least part of the X-ray flux originates within the binary system.

The present work develops a general expanding source model, and then analyzes the implications of this model for SS 433. First, in § II we provide a systematic treatment of nonrelativistic expanding sources entrained in jets, including continuous electron injection and X-ray emission by inverse Compton scattering. The methodology is based on the nonthermal models found in Band and Grindlay (1985, 1986; hereafter BG85, BG86, respectively). The model focuses on a number of aspects of the expanding source: the evolution of the observable quantities (§ II*a*); the electron density, magnetic field, and size of a spherical source based on observation (§ II*b*); and the physics that affects the source evolution (§ II*c*). In addition, we describe free-free absorption internal and external to the expanding source (§ II*d*).

In § III, the expanding source model is applied to SS 433. Quantitative source models with X-ray production by inverse Compton scattering are shown to be far out of equipartition, while a model assuming equipartition can only produce the radio flux and yet satisfies both observational and modeling constraints (§ III*a*). After the consideration of a number of modifications to the source model in § III*b*, we conclude that the X-rays most likely do not originate in the expanding source and that another X-ray source is required. Nontheless, the evolution of the radio flares provides information about the expanding source (§ III*c*).

The conclusion in § III*b* that the X-rays from SS 433 do not originate out in the jets leads us to suggest in § IV that the X-rays are produced by a compact nonthermal source within the binary system. The resulting source morphology is very similar to the AGN model proposed by BG86: radio emission from the jets and X-rays produced in a compact central nonthermal source by inverse Compton scattering of optical-ultraviolet photons from the central engine. In SS 433 the synchrotron emission is masked by other sources of infrared and optical emission.

Finally in § V we summarize our results.

II. MODEL FOR EXPANDING SOURCE

We model the source as a region of nonthermal electrons (and perhaps thermal gas) with characteristic dimension r at a distance R from the central object which is presumably the origin of the emitting region. In SS 433 the expanding region is the "plasmon" (SGJG), and central object is the compact member of the binary. We will be concerned mainly with spherical sources (in which case r is the source radius), but we include some discussion of other shapes. The geometry is sketched in Figure 1. The electrons radiate synchrotron photons in a homogeneous, tangled magnetic field B, and scatter photons produced by both the external central object and the synchrotron process. Thus we do not consider the polarization of the nonthermal emission in our model.

a) Expansion

Since most of the physical quantities vary as a power law of the source dimensions, we can parameterize them in terms of the expanding dimension at a fiducial time t_0 [for any quantity X, $X(t_0) = X_0$]. We define χ as $r = \chi r_0$, where r is the expanding dimension. As will be discussed below, we assume that the distance from the central object R scales linearly with the expanding dimension. Table 1 presents the parameterization of the physical quantities for both the general and spherically symmetric cases. Since most quantities evolve as a power of the expanding dimension, we parameterize them as power laws of χ. Likely values of the power-law indices are discussed below in § II*c*. A factor $F(\chi)$ in the electron distribution $dn_e = n_0 \gamma^{-p} \chi^{-z} F(\chi) d\gamma \, [\gamma_{\min}(t) \leq \gamma \leq \gamma_{\max}(t)]$ allows for electron injection.

Note that the average photon path length within the source r_s (i.e., not necessarily along the line of sight), as well as the average path length along the line of sight l, will increase linearly with r for spherical expansion but will increase in a more complicated manner for other types of expansion. For example, if a thick disk with expanding radius is viewed along its normal, the average line of sight l will remain constant, but the average path length r_s will increase roughly in proportion to the radius. This distinction is important since the effect of absorption on the observable spectrum is proportional to the line of sight within the source, while processes proportional to the average photon density, such as inverse Compton scattering, scale with the average path length. The actual variation of each of these path lengths as the source expands depends on the model for the particular object and the viewing angle assumed. Here we merely parameterize these quantities as $l = l_0 \chi^{e_1}$ for the line of sight and $r_s = r_{s_0} \chi^{e_2}$ for the average path length.

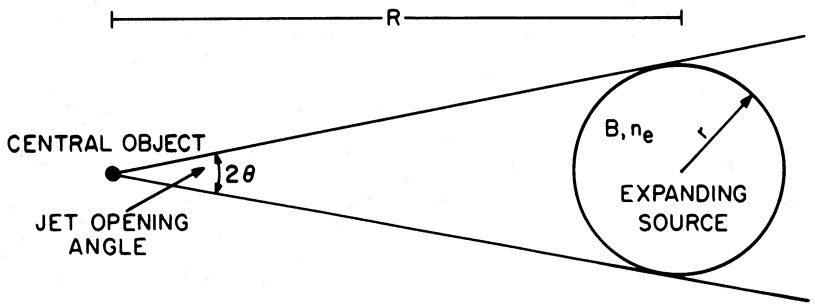

FIG. 1.—Sketch of the geometry assumed in the model. Note that in sources with two-sided jets there may be two expanding sources.

TABLE 1

PARAMETERIZATION

Quantity	Parameterization	Spherical Expansion
Source dimension r	χ	χ
Distance from central object R	χ	χ
Volume V	χ^{d}	χ^{3}
Magnetic field B	χ^{-m}	χ^{-2}
Electron energy γ	χ^{-g}	χ^{-1}
Electron density n_{e0}	$\chi^{-z}F(\chi)$	$\chi^{-3-2\alpha}$
Line of sight l	χ^{e_1}	χ
Photon path length r_s	χ^{e_2}	χ
Optical thin synchrotron luminosity $L^s_{\nu\,\mathrm{thin}}$	$\chi^{-z-m(1+\alpha)+d}F(\chi)$	$\chi^{-2-4\alpha}$
Synchrotron optical depth τ_s	$\chi^{e_1-z-m(\alpha+3/2)}F(\chi)$	$\chi^{-5-4\alpha}$
Optical thick synchrotron luminosity $L^s_{\nu\,\mathrm{thick}}$	$\chi^{d-e_1+m/2}$	χ^{3}
Synchrotron frequency ν_T	$\chi^{[e_1-z-m(\alpha+3/2)]/(\alpha+5/2)}F(\chi)$	$\chi^{(-5-4\alpha)/(\alpha+5/2)}$
Peak synchrotron luminosity L^p_ν	$\chi^{[(\alpha+5/2)d-(e_1+2m)-5/2(z+m)]/(\alpha+5/2)}F(\chi)^{5/(2\alpha+5)}$	$\chi^{(-5-7\alpha)/(\alpha+5/2)}$
Compton optical depth τ_C	$\chi^{e_2-z}F(\chi)$	$\chi^{-2-2\alpha}$
SSC L^c_ν	$\chi^{e_2+d-2z-m(1+\alpha)}F(\chi)^2O(1)$	$\chi^{-4-6\alpha}O(1)$
IC L^c_ν	$\chi^{d-3+e_2-z}F(\chi)$	$\chi^{-2-2\alpha}$

Having parameterized the physical quantities, we now find how the observables scale with expansion. The optically thin synchrotron luminosity is

$$L^s_{\nu\,\mathrm{thin}} = C_\alpha n B^{1+\alpha}\nu^{-\alpha}V = L^s_{\nu 0\,\mathrm{thin}}\chi^{-z-m(1+\alpha)+d}F(\chi)\,, \tag{II.1}$$

where $\alpha = (p-1)/2$ and $C_\alpha = 2.707\times 10^{-22}(2.799\times 10^6)^\alpha j_{\alpha 0}$. The observed synchrotron optical depth is

$$\tau_s = \kappa_\alpha B^{\alpha+3/2} n \nu^{-(\alpha+5/2)} l = \tau_{s0}\chi^{e_1-z-m(\alpha+3/2)}F(\chi)\,, \tag{II.2}$$

where $\kappa_\alpha = 1.978\times 10^7(2.799\times 10^6)^\alpha k_{\alpha 0}$ and $e_1 = 1$ if the dimension along the line of sight expands. The constants $j_{\alpha 0}$ and $k_{\alpha 0}$ are from Jones, O'Dell, and Stein (1974). The asymptotic optically thick spectrum is

$$L^s_{\nu\,\mathrm{thick}} = \frac{a}{\tau_s}L^s_{\nu\,\mathrm{thin}} = L^s_{\nu 0\,\mathrm{thick}}\chi^{d-e_1+m/2}\,, \tag{II.3}$$

where a is a geometric factor; $a = \frac{3}{4}$ for a sphere (BG85). The shape of the spectrum in the vicinity of the turnover is geometry dependent and can deviate substantially from the asymptotic limits for a few frequency decades below the turnover for an inhomogeneous source (see BG85). If we define the turnover frequency ν_T as $\tau_s(\nu_T) = 1$, then

$$\nu_T = (\kappa_\alpha B^{\alpha+3/2} n l)^{1/(\alpha+5/2)} = \nu_{T0}\chi^{[e_1-z-m(\alpha+3/2)]/(\alpha+5/2)}F(\chi)^{1/(\alpha+5/2)}\,. \tag{II.4}$$

The frequency of the peak of the spectrum is proportional to this turnover frequency (see BG86). Thus the peak spectral luminosity is

$$L^p_\nu = L^p_{\nu 0}\chi^{[(\alpha+5/2)d-(e_1+2m)\alpha-5/2(z+m)]/(\alpha+5/2)}F(\chi)^{5/(2\alpha+5)}\,. \tag{II.5}$$

The relativistic electrons in the source can scatter both synchrotron photons produced within the source and photons emitted from the central source. As was presented in BG86, the inverse Compton scattering of the synchrotron photons is

$$L^c_\nu = L^s_\nu \tau_C \frac{9}{8}\alpha A(\alpha)\ln\frac{\nu_h}{\nu_T}\,, \tag{II.6}$$

where $A(\alpha)$ is a spectral index dependent factor of order unity, ν_h is the high-frequency synchrotron cutoff, and τ_C is the average Compton optical depth, given by

$$\tau_C = n_e\sigma_T r_s = \tau_{c0}\chi^{e_2-z}F(\chi)\,, \tag{II.7}$$

where e_2 allows for expansion of the average path length within the source (scattering *into* the line of sight is proportional to the average path length). For calculating the scattering *out* of the line of sight e_2 should be replaced by e_1, the index for the path length along the line of sight. The high-frequency synchrotron cutoff is

$$\nu_h \approx 2.1\times 10^6\gamma^2_{\max}B = \nu_{h0}\chi^{-m-2g}\,. \tag{II.8}$$

Thus, the scattered flux is

$$\begin{aligned} L^c_\nu &= L^s_\nu\left(\frac{L^c_{\nu 0}}{L^s_{\nu 0}}\right)\chi^{e_2-z}F(\chi)\left\{1+\frac{[z-m-e_2-2g(\alpha+5/2)]\ln(\chi)-\ln F(\chi)}{(\alpha+5/2)\ln(\nu_{h0}/\nu_{T0})}\right\} \\ &= L^c_{\nu 0}\chi^{e_2+d-2z-m(1+\alpha)}F(\chi)^2\left\{1+\frac{[z-m-e_2-2g(\alpha+5/2)]\ln(\chi)-\ln F(\chi)}{(\alpha+5/2)\ln(\nu_{h0}/\nu_{T0})}\right\}. \end{aligned} \tag{II.9}$$

If the spectral luminosity (luminosity per Hz) of the central source is L_ν^0, then the photon density (assuming $r/R \ll 1$) within the emitting region is $n_\nu = (L_\nu^0/h\nu)(1/4\pi cR^2)$ (BG86). The scattered luminosity is then

$$L_\nu^c = \tau_C \frac{3V}{8\pi R^2 r} \alpha A(\alpha) \nu^{-\alpha} \int_0^\infty d\nu' \nu'^{\alpha-1} L_\nu^0(\nu') = L_{\nu 0}^c \chi^{d-3+e_2-z} F(\chi) . \tag{II.10}$$

The central source may have a thermal spectrum with total luminosity L

$$L_\nu^0 = \left(\frac{\nu}{\nu_T}\right)^z \left[\frac{L}{\nu_T J(1+z)}\right] \left[\exp\left(\frac{\nu}{\nu_T}\right) - 1\right]^{-1} , \tag{II.11}$$

where

$$J(s) = \int_0^\infty d\xi \xi^{s-1} [\exp(\xi) - 1]^{-1} = \Gamma(s)\zeta(s) , \qquad s > 1 ,$$

is a commonly occurring normalization factor (expressible as the product of the gamma and Riemann zeta functions), and $\nu_T = 2.0836 \times 10^{10} T$ is the frequency corresponding to temperature T. For a spherically expanding source the scattered flux is

$$L_\nu^c = \frac{\tau_C \alpha A(\alpha)}{2} \left(\frac{r}{R}\right)^2 \nu^{-\alpha} I , \tag{II.12}$$

where

$$I = \int_0^\infty d\nu' \nu'^{\alpha-1} L_\nu^0(\nu') = \int_0^\infty d\nu' \nu'^{\alpha-1} \left(\frac{\nu'}{\nu_T}\right)^z \left[\frac{L}{\nu_T J(1+z)}\right] \left[\exp\left(\frac{\nu'}{\nu_T}\right) - 1\right]^{-1} = \frac{L\nu_T^{\alpha-1} J(\alpha+z)}{J(1+z)} .$$

A value of $z = 3$ corresponds to a single-temperature blackbody, while $z = 4/3$ corresponds to $L_\nu \propto \nu^{-1/3}$ expected from an accretion disk cutoff by an exponential (see BG86). Table 2 provides $J(\alpha + z)$ as a function of α for $z = 4/3$ and $z = 3$.

b) *Fiducial Values of Physical Parameters*

The physical quantities at a given time are necessary to complete the descriptive model. Here we consider spherical sources only. We assume that the radio observations are sufficient to determine the spectral index $\alpha = (p - 1)/2$, the optically thin spectral

TABLE 2

THERMAL NORMALIZATION FUNCTIONS $J(\alpha + z)$

α	$z = 4/3$	$z = 3$
0.00.....	3.16792	2.40409
0.05.....	2.82757	2.49871
0.10.....	2.56737	2.60061
0.15.....	2.36454	2.71027
0.20.....	2.20408	2.82820
0.25.....	2.07577	2.95496
0.30.....	1.97244	3.09116
0.35.....	1.88999	3.23745
0.40.....	1.82164	3.39458
0.45.....	1.76761	3.56331
0.50.....	1.72477	3.74452
0.55.....	1.69151	3.93913
0.60.....	1.66658	4.14815
0.65.....	1.64899	4.37268
0.70.....	1.63798	4.61393
0.75.....	1.63296	4.87320
0.80.....	1.63347	5.15189
0.85.....	1.63915	5.45157
0.90.....	1.64973	5.77389
0.95.....	1.66501	6.12068
1.00.....	1.68485	6.49393
1.05.....	1.70918	6.89580
1.10.....	1.73795	7.32864
1.15.....	1.77117	7.79501
1.20.....	1.80888	8.29772
1.25.....	1.85117	8.83980
1.30.....	1.89814	9.42456
1.35.....	1.94993	10.05564
1.40.....	2.00673	10.73697
1.45.....	2.06874	11.47288
1.50.....	2.13619	12.26806

luminosity L_s (presumably due to synchrotron emission) at a reference radio frequency, and the synchrotron optical depth τ_s at that frequency. In addition, we assume that the X-ray spectral luminosity L_c is known at a reference X-ray frequency. The source is modeled as a sphere with radius $r = R\theta$ at a distance R (which might be determined by VLBI) from the central object.

We consider three different X-ray origins. In two cases the X-rays originate in the expanding source, either from inverse Compton scattering of soft photons from the central object (this case will be labeled "IC") or from synchrotron–self-Compton scattering of synchrotron photons (labeled "SSC") emitted within the source. In the third case the X-ray flux originates in another source; since in this case there are fewer observations constraining the model, we assume equipartition. The various processes can be parameterized as follows:

$$L_s = C_1 n B^{1+\alpha} R^3 \theta^3 , \quad \text{synchrotron emission;}$$

$$\tau_s = C_2 n B^{\alpha+3/2} R\theta , \quad \text{synchrotron optical depth;}$$

and one of the following three equations:

$$L_c = C_3 n R\theta^3 , \quad \text{IC;}$$

or

$$L_c = C_4 n^2 B^{1+\alpha} R^4 \theta^4 , \quad \text{SSC;} \tag{II.13}$$

or

$$n = C_5 B^2 , \quad \text{equipartition .}$$

The constants C_1, C_2, C_3, C_4, and C_5 are given in Table 3. The constant C_3 is a function of the luminosity and temperature of the central object's thermal source. Note that in the IC case the distance from the central object R is necessary to calculate the physical parameters, while in the other two systems it occurs only in the calculated quantity $R\theta$ (which is the source radius).

If inverse Compton scattering dominates, then the resulting parameters are

IC case:

$$n = \left(\frac{C_1}{L_s}\right)^{(6\alpha+9)/4(\alpha+1)} \left(\frac{L_c R^2}{C_3}\right)^{(4\alpha+7)/4(\alpha+1)} \left(\frac{\tau_s}{C_2}\right)^{3/2} ,$$

$$B = \left(\frac{L_s C_3}{C_1 L_c R^2}\right)^{1/(1+\alpha)} , \tag{II.14}$$

$$\theta = \left(\frac{L_s}{C_1 R^2}\right)^{(2\alpha+3)/4(\alpha+1)} \left(\frac{C_3}{L_c}\right)^{1/4(\alpha+1)} \left(\frac{C_2}{\tau_s}\right)^{1/2} .$$

On the other hand, if the SSC scattering dominates, the resulting parameters are

SSC case:

$$n = \left(\frac{C_1}{L_s}\right)^{(3\alpha+5)/(2\alpha+3)} \left(\frac{\tau_s}{C_2}\right)^{(\alpha+1)/(2\alpha+3)} \left(\frac{L_c}{C_4}\right)^{(2\alpha+7/2)/(2\alpha+3)} ,$$

$$B = \left(\frac{\tau_s C_4 L_s}{C_2 L_c C_1}\right)^{1/(\alpha+3/2)} , \tag{II.15}$$

$$R\theta = \left(\frac{L_s}{C_1}\right)^{(\alpha+2)/(2\alpha+3)} \left(\frac{C_2}{\tau_s}\right)^{(\alpha+1)/(2\alpha+3)} \left(\frac{C_4}{L_c}\right)^{1/(4\alpha+6)} .$$

TABLE 3

CONSTANTS FOR FIDUCIAL VALUES

Parameter	Explosion
C_1.....	$1.1339 \times 10^{-21}(2.7992 \times 10^{-3})^{\alpha} j_{\alpha 0}(\nu_r/\mathrm{GHz})^{-\alpha}$
C_2.....	$6.2556 \times 10^{-16}(2.7992 \times 10^{-3})^{\alpha} k_{\alpha 0}(\nu_r/\mathrm{GHz})^{-(\alpha+5/2)}$
C_3.....	$470.28(8.617 \times 10^{-4})^{\alpha} A(\alpha) J(\alpha+z) \dfrac{(L/10^6\ L_\odot)}{(T/10^4\ \mathrm{K})^{1-\alpha}} \left(\dfrac{\nu_x}{\mathrm{keV}}\right)^{-\alpha}$
C_4.....	$9.770 \times 10^{-46}(1.1577 \times 10^{-11})^{\alpha} A(\alpha) j_{\alpha 0}(\nu_x/\mathrm{keV})^{-\alpha} N_\nu$
C_5.....	$\dfrac{(2\alpha-1)\gamma_{\min}^{2\alpha-1}}{8\pi mc^2[1-(\gamma_{\max}/\gamma_{\min})^{1-2\alpha}]} = 4.8598 \times 10^4 \dfrac{\gamma_{\min}^{2\alpha-1}}{[1-(\gamma_{\max}/\gamma_{\min})^{1-2\alpha}]}$

NOTE.—The quantities ν_r and ν_x are the reference synchrotron and scattered frequencies, respectively; $j_{\alpha 0}$ and $k_{\alpha 0}$ are the isotropic synchrotron emissivity and absorptivity constants defined in Jones, O'Dell and Stein 1974; L, T, and $J(\alpha+z)$ due to the thermal source are discussed in eq. (II.11); $A(\alpha)$ is a spectral index factor of order unity defined in BG86; N_ν is the number of frequency decades over which the optically thin synchrotron spectrum extends; and $\gamma_{\min}$ is the low-energy cutoff of the electron distribution.

Finally, if the X-ray emission is produced by another source and we assume equipartition instead, then the physical parameters are

Equipartition:

$$n = \left(\frac{\tau_s}{C_2}\right)^{12/(4\alpha+15)} \left(\frac{C_1}{L_s}\right)^{4/(4\alpha+15)} C_5^{(4\alpha+7)/(4\alpha+15)} ,$$

$$B = \left(\frac{\tau_s}{C_2}\right)^{6/(4\alpha+15)} \left(\frac{C_1}{L_s}\right)^{2/(4\alpha+15)} C_5^{-4/(4\alpha+15)} , \tag{II.16}$$

$$R\theta = \left(\frac{C_2}{\tau_s}\right)^{(2\alpha+6)/(4\alpha+15)} \left(\frac{L_s}{C_1}\right)^{(2\alpha+7)/(4\alpha+15)} C_5^{-1/(4\alpha+15)} .$$

c) *Physics of Source Parameters*

The model above only describes the emissions and evolution of an expanding source. While a full dynamical model is not treated here, a number of significant dynamical aspects are discussed in what follows.

i) *Expansion*

We assume throughout that the source expands uniformly, $r = r_0 + ut$, as it travels at constant velocity away from the origin, $R = R_0 + Vt$, where $t = 0$ at the fiducial point used for the parameterization in § II*a*. The fiducial time $t_0 = r_0/u$ is thus the (extrapolated) time for r to expand from 0 to r_0. Note that $\chi = 1 + t/t_0$. Since the source does not actually expand from zero radius, the flare begins later than $t = -t_0$. While the jet opening angle $\theta = r/R$ will not be constant if $R_0/r_0 \neq V/u$, it approaches a constant value $\theta = u/V$ asymptotically. For purposes of simplicity we will assume that θ is constant.

ii) *Inhomogeneities*

We assumed above that the source is a single homogeneous sphere. However, it is possible that the emitting plasma is clumped and should be modeled as many smaller sources within the emission region. Band (1987) considers this possibility in greater depth; here we only summarize the results. If N is the number of emitting sources within a spherical region of radius r, and the radius of an individual source is ηr, then $f = N\eta^3$ is the filling factor. Whether by synchrotron or scattering processes, photon emission is proportional to the total number of nonthermal electrons, and thus to the filling factor. However, the synchrotron optical depth and the SCC scattered emission are both proportional to the electron column density the photons traverse which consists not only of the average column density through the entire region but also the column density through the dense emitting source. Thus the column density is proportional to $1 + \eta/f$ and is enhanced when $f \ll \eta$. The effects of clumping on the emission cases of equations (II.13)–(II.16) can be included if the constants are modified as follows:

$$C_1' = fC_1 , \qquad C_2' = (\eta + f)C_2 , \qquad C_3' = fC_3 , \qquad C_4' = f(\eta + f)C_4 , \tag{II.17}$$

where primed (unprimed) quantities are the clumped (unclumped) constants. Since clumping always increases the electron density but only decreases the magnetic field, the ratio of electron to magnetic field energy densities always increases with clumping (Band 1987).

iii) *Magnetic Field*

The evolution of the magnetic field depends on the type of expansion and the nature of the flows within the source. Vitello and Salvati (1976) showed that if the magnetic field energy density is insignificant in comparison to the particle fields (relativistic or thermal) and the source is not turbulent, then the quantity $B_\perp^2 B_\parallel/\rho^2$ is constant along flow lines, where $B_\perp$ and $B_\parallel$ are the magnetic field components perpendicular and parallel, respectively, to the direction of expansion and ρ is the density of the material threaded by the magnetic field. A consequence of this is that the different components of the magnetic field are comparable for homologous spherical expansion and vary as $B \propto \chi^{-2}$ (Vitello and Pacini 1977), and the magnetic field index (defined in Table 1) $m = 2$ as assumed by van der Laan (1966). Other types of expansion can result in different dependencies on χ of the magnetic field components. For example, in expansion along one dimension $B_\parallel$ remains constant while $B_\perp \propto \chi^{-1}$, so that eventually $B_\parallel \gg B_\perp$ (Vitello and Pacini 1977).

While it provides a reasonable initial approximation, this relation between the components of B and ρ derived by Vitello and Salvati (1976) may not be valid in many sources where the magnetic field energy density may be large and the plasma turbulent. An alternative is to assume that the electron and magnetic fields are in equipartition, as might be expected if the plasma is turbulent and electrons are accelerated by processes involving the magnetic field. Thus $\chi^{-m} = \chi^{-z/2} F(\chi)^{1/2}$. Consequently the optically thick flux is no longer independent of $F(\chi)$, and the evolution of the source is impossible to decipher without more sophisticated models of the source physics (e.g., the electron injection mechanism) or recourse to more detailed observation.

iv) *Electron Distribution*

In the context of the expanding source model presented in §§ II*a*, *b* adiabatic expansion, radiative losses (either synchrotron or inverse Compton), and physical escape must be considered among the possible loss mechanisms that affect the electron distribution. The following are the time scales of these processes and their dependence on the expansion of the source (the power law indices d, g,

m, and z are defined in Table 1):

Adiabatic: $$T_a = \frac{t_0}{g}\chi = T_{a0}\chi .$$

Synchrotron: $$T_s = \frac{3 \times 10^8}{\gamma(B \sin \phi)^2} = T_{s0}\chi^{2m} .$$

Compton scattering: $$T_{CS} = \frac{1.2 \times 10^7}{\gamma u_{ph}} . \tag{II.18}$$

SSC: $$T_{SSC} = T_{SSC0}\chi^{z+d-2+2[m+g(1-\alpha)]}F(\chi)^{-1}O(1) .$$

IC: $$T_{IC} = T_{IC0}\chi^2 .$$

Escape: $$T_{es} = \frac{R}{v_e} = T_{es0}\chi .$$

The adiabatic cooling time scale assumes uniform expansion. The radiative loss time scales T_s, T_{SSC}, and T_{IC} are for electrons at an energy γ and thus does not include the energy decrease of a given electron due to adiabatic losses. A factor of order unity due to the change of the cutoffs of the optically thin synchrotron spectrum has been dropped in the expression for T_{SSC}. The characteristic velocity of electrons through the source v_e may be less than the speed of light due to diffusion. Note that at large times (e.g., large χ) adiabatic losses and physical escape will dominate the radiative loss mechanisms. Since the acceleration of nonthermal electrons is still poorly understood, the dependence of the injection of nonthermal electrons on the physical parameters is less certain and is usually determined empirically.

The electron distributions and the observable spectra that result from these injection and loss mechanisms have been discussed elsewhere (e.g., Kardashev 1962; Tucker 1975). Here we will only comment on a few relevant distributions of interest in our models.

The energy density for adiabatic expansion of the relativistic electrons varies as $u \propto n_e^{4/3}$, where n_e is the number of density of relativistic electrons (Vitello and Salvati 1976). The energy density due to electrons with energy γ is $u_\gamma \propto n_e\gamma$. Thus $\gamma \propto n_e^{1/3} \propto \chi^{-d/3}$ and the index $g = d/3$ (see Table 1). Thus an electron distribution that loses energy due to adiabatic expansion alone evolves as

$$dn_e = n_0\gamma^{-p}\chi^{-d-g(p-1)}d\gamma , \tag{II.19}$$

and the index $z = d + g(p-1) = d(1 + 2/3\alpha)$ and $F(\chi) = 1$. If electrons are injected into the source at the rate $q(t)\gamma^{-p}$, the resulting electron distribution is

$$n = \gamma^{-p}\chi^{-d-g(p-1)}\left[n_0 + \frac{1}{V_0}\int_0^t \left(\frac{t_0}{\tau + t_0}\right)^{-g(p-1)} q(\tau)d\tau\right] = n_0\gamma^{-p}\chi^{-z}F(\chi) ,$$

$$F(\chi) = 1 + \frac{t_0}{V_0 n_0}\int_1^\chi \lambda^{g(p-1)}q[t_0(\lambda - 1)]d\lambda, \quad \text{and} \quad z = d\left(1 + \frac{2}{3\alpha}\right), \tag{II.20}$$

where V_0 is the source volume and n_0 the electron density at the fiducial time. Peterson and Dent (1973) used a similar distribution to model flares from 3C 273. Note that $F(\chi)$ cannot decrease with χ.

Since the electron lifetime due to radiative losses decreases with energy, the electron distribution may be steeper at high energy than the injected distribution. For example, if electrons are injected continuously with a power-law distribution $\propto\gamma^{-p}$, radiative losses will modify the high-energy distribution to $\propto\gamma^{-p-1}$. At low energies a loss mechanism with an energy-independent electron lifetime (such as adiabatic losses or escape from the emission region) might dominate the radiative losses, maintaining the injected γ^{-p} distribution. The electron distribution will then be $\propto\gamma^{-p}$ at low energy and $\propto\gamma^{-p-1}$ at high energy, with a resulting nonthermal spectrum $\propto\nu^{-(p-1)/2}$ at low frequency and $\propto\nu^{-p/2}$ at high frequency. At the break energy between the high- and low-energy power laws the electron lifetimes due to the two loss mechanisms are approximately equal. This two-part power-law distribution is used in many source models (e.g., Marscher and Brown 1975; Königl 1981; BG86) including the compact source model for SS 433 described in § IV.

In expanding sources the radiative loss time scale increases more rapidly with χ than the time scales of adiabatic loss or physical escape, and thus the break energy increases with time *if there is continuous injection.* However, if no additional electrons are injected, then initially synchrotron losses cause a break in the electron distribution, and subsquently adiabatic losses shift this break down in energy (see Kardashev 1962). In this case the break energy decreases with time (as opposed to the increase found by Marscher and Brown 1975). In addition, because of the dependence of synchrotron radiation on pitch angle, the evolution and shape of the electron distribution and its synchrotron emissions must be treated with care when synchrotron losses dominate (Kardashev 1962; Tucker 1975).

d) Free-Free Absorption

Thermal gas either in the emitting region or in front of it can also absorb photons by free-free absorption (Marscher and Brown 1975). The absorptivity is (Tucker 1975; Rybicki and Lightman 1979)

$$\kappa_{th} = 1.39 \times 10^{-8} n_{th}^2 \left(\frac{T}{10^4\ \mathrm{K}}\right)^{-3/2} \nu^{-2}\left[31.366 + 1.5 \ln\left(\frac{T}{10^4\ \mathrm{K}}\right) - \ln \nu\right], \tag{II.21}$$

where T is the temperature of the gas, $n_{\rm th}$ is the density of thermal electrons and protons, and we use the average ion charge $\langle \sum_i N_e N_i Z_i^2 \rangle = 1.4 N_e^2$ (N_e is the electron density, N_i the ith ion density, and Z the ion charge). Note that we differ with Marscher and Brown (1975) on the value of some of the constants. The Gaunt factor used in equation (II.21) is valid for $T < 4 \times 10^5$ K and $\nu < 10^{12}(T/10^4\ {\rm K})^{3/2}$ (Tucker 1975). If the gas is isothermal (as was assumed by Marscher and Brown 1975), then the absorptivity decreases due to the decrease of the density, and $\kappa_{\rm th} \propto \chi^{-2d}$. However, if the gas expands adiabatically, as would be expected if the relativistic particles expand adiabatically, then the decrease in the temperature must also be considered. For adiabatic changes $T \propto \rho_{\rm th}^{\gamma-1}$, where $r_{\rm th}$ is the density of the thermal gas and γ is the adiabatic index. For a nonrelativistic gas $\gamma = 5/3$. Hence $T \propto \rho_{\rm th}^{2/3} \propto \chi^{-2d/3}$ and $\kappa_{\rm th} \propto \chi^{-d}$, where we have neglected the temperature change in the logarithm.

If there is free-free absorption within the source, then the optical depth τ_s in equation (II.2) must be replaced by

$$\tau = (\kappa_s + \kappa_{\rm th})l = [\kappa_{s0}\chi^{-z-m(3/2+\alpha)}F(\chi) + \kappa_{\rm th0}\chi^{-ad}]l_0\chi^{e_1}\ , \tag{II.22}$$

where $a = 1$ for adiabatic thermal expansion and $a = 2$ for isothermal expansion. The observed optically thick spectrum will have an algebraic frequency dependence flatter than the optically thick synchrotron spectrum.

If the absorbing material is in front of the source, then the spectrum will be rapidly cutoff below the frequency at which the optical depth is unity: absorption contributes a factor $\exp(-\tau)$ and $\tau \propto \nu^{-2}$ (ignoring the logarithmic dependence on frequency in the absorption). The evolution of this absorption will depend on the assumed distribution of the thermal gas outside the expanding source and the source geometry, which can only be calculated for models of specific objects.

III. THE FLARES FROM SS 433

The expanding source methodology developed in the previous section consists of two components: the evolution of the expanding source and its emissions; and the values of the source parameters at a fiducial time. Following SGJG, in this section we analyze radio and X-ray observations from SS 433 as nonthermal emissions from an expanding source entrained in the jets. We use contemporaneous radio–X-ray data reported by SGJG (the X-ray observations were reanalyzed in GB84) that track two flares from SS 433. First, we will calculate the physical parameters of the source from radio and X-ray observations at two epochs and check the resulting model for consistency. We find that the X-rays most probably do not originate in the expanding sources; in § IV we suggest an alternative origin. Finally, the source evolution is determined from the radio observations.

a) Physical Parameters of the Expanding Source

Quantitative models of the expanding source can be calculated from the simultaneous radio and X-ray observations of SGJG and GB84 using the methodology of equations (II.14)–(II.16) with the three different assumptions about the origin of the X-rays. The X-rays may be produced by inverse Compton scattering of photons from the binary (the IC model), by scattering of synchrotron photons from within the source (the SSC model), or by another (as yet undetermined) source in which case we assume equipartition to constrain the model (the equipartition model). In these models we assume the radio turnover results from synchrotron self-absorption; the entire X-ray flux originates from the flaring component (whether or not it is produced in the expanding source); and the distance R from the central object (see Fig. 1) is the distance the plasma entrained in the jets traveled at a velocity of $0.26c$ since the flare began (this is found below in § III*c*).

Although the jets of SS 433 are only mildly relativistic ($v = 0.26c$, $\gamma_{\rm jet} = 1.036$), the relativistic effects are sufficient to amplify the emissions from the approaching jet relative to the receding jet by a factor of 2.55 for the flare under consideration, where we used the orientation of the jets at the time the flare began (presumably when the plasma was injected into the jets). In constructing our models we use optical depths and relativistically corrected flux densities for the approaching source alone (i.e., we neglect the receding source). However, there are only small differences between models calculated with and without the relativistic correction where the emissions come from one or two sources.

We use a single-temperature thermal source within the binary system with a luminosity of 2.6×10^{39} ergs s^{-1} and a temparature of 4×10^4 K, consistent with the observations of Wagner (1983, 1986). While these numbers differ from the best fit of Wagner (1986), they fall within the range of acceptable values (although for this temperature this luminosity may be about a factor of 2 too low compared to the best-fit relationship between temperature and luminosity). Modeling the optical source as a single-temperature blackbody is clearly a simplification given its likely origin: a luminous star or an accretion disk. In addition, the emissions in the infrared through ultraviolet bands most likely originate in a number of different sources. Analysis of the primary and secondary optical minima led Cherepashchuk (1981) to conclude that the companion emits about half the optical luminosity of the source surrounding the compact object. Free-free emission from an ionized plasma within the binary system has been suggested as a source of the infrared flux (Giles *et al.* 1979; Wynn-Williams and Becklin 1979), although the discovery of weak precession and orbital variations in the infrared data suggests that a number of different sources contribute to the observed flux (Catchpole *et al.* 1981). Preliminary *IRAS* pointed observations flux densities of 0.35 Jy at 12 μm and 0.19 Jy at 25 μm (signal to noise of $\sim$10–15; Gillett 1985, private communication) indicate that there is significant excess thermal emission into the far-infrared. Further, the large absorption—$A_V \approx 8$—is still not well determined (Murdin, Clark, and Martin 1980; Margon 1984; see GB84 for a discussion of the related X-ray absorption), complicating the spectral fits. However, the inverse Compton scattering flux is relatively insensitive to the details of the soft photon spectrum (BG85, BG86), and approximating the thermal spectrum as a single-temperature blackbody suffices. Because of the approximate nature of the optical source used in our calculations, we have not included relativistic corrections resulting from the motion of the scattering electrons away from the central object.

Table 4 presents the resulting models at two different epochs for the first of the two flares observed by SGJG. These models show that if the observed X-rays are indeed produced within the expanding source, the IC and SSC processes both contribute significant fractions of the X-ray flux. In the equipartition model the X-ray fluxes from both the IC and SSC processes are far fainter than the

TABLE 4

MODELS OF SS 433 FLARE

A.

	OBSERVED			ACTUAL				
t	S_r	τ_s	S_x	S_r	τ_s	S_x	R	ν_h
5.21.....	1.15×10^{-23}	6.25	9.42×10^{-29}	7.92×10^{-24}	8.62	6.48×10^{-29}	2.13×10^{15}	10^{13}
8.09.....	1.05×10^{-23}	0.70	1.28×10^{-28}	7.23×10^{-24}	0.966	8.53×10^{-29}	4.07×10^{15}	10^{13}

B.

	$t = 5.21$			$t = 8.09$		
MODEL	IC	SSC	Equipartition	IC	SSC	Equipartition
n.....	5.51×10^{10}	2.80×10^{10}	4.72×10^{3}	2.48×10^{10}	1.76×10^{10}	1.07×10^{3}
B	6.85×10^{-4}	9.15×10^{-4}	6.97×10^{-1}	2.43×10^{-4}	2.81×10^{-4}	3.31×10^{-1}
r.....	1.26×10^{-2}	1.35×10^{-2}	7.10×10^{-2}	2.77×10^{-2}	2.87×10^{-2}	1.68×10^{-1}
θ^R	5.90×10^{-3}	6.34×10^{-3}	3.33×10^{-2}	6.80×10^{-3}	7.06×10^{-3}	4.13×10^{-2}
$\theta°$.....	0.34	0.36	1.91	0.39	0.40	2.37
S_x IC	6.48×10^{-29}	4.08×10^{-29}	9.99×10^{-34}	8.53×10^{-29}	6.74×10^{-29}	8.22×10^{-34}
S_x SSC	1.19×10^{-28}	6.48×10^{-29}	5.74×10^{-35}	1.16×10^{-28}	8.54×10^{-29}	3.04×10^{-35}
u_B	1.87×10^{-8}	3.33×10^{-8}	1.93×10^{-2}	2.34×10^{-9}	3.15×10^{-9}	4.36×10^{-3}
u_e.....	2.26×10^{5}	1.15×10^{5}	1.93×10^{-2}	1.02×10^{5}	7.19×10^{4}	4.36×10^{-3}
u_γ SSC	1.12×10^{-3}	9.68×10^{-4}	3.50×10^{-5}	2.30×10^{-4}	2.14×10^{-4}	6.24×10^{-6}
u_γ IC	1.52×10^{-3}	1.52×10^{-3}	1.52×10^{-3}	4.16×10^{-4}	4.16×10^{-4}	4.16×10^{-4}
γ(1 GHz)	834	722	26.1	1400	1300	37.9
γ(25 GHz).....	4170	3610	131	7000	6510	190
T_a.....	2.7×10^{5}	2.7×10^{5}	2.7×10^{5}	5.2×10^{5}	5.2×10^{5}	5.2×10^{5}
T_s.....	$2.6 \times 10^{15}\gamma^{-1}$	$1.4 \times 10^{15}\gamma^{-1}$	$2.5 \times 10^{9}\gamma^{-1}$	$2.0 \times 10^{16}\gamma^{-1}$	$1.5 \times 10^{16}\gamma^{-1}$	$1.1 \times 10^{10}\gamma^{-1}$
T_{IC}.....	$7.9 \times 10^{9}\gamma^{-1}$	$7.9 \times 10^{9}\gamma^{-1}$	$7.9 \times 10^{9}\gamma^{-1}$	$2.9 \times 10^{10}\gamma^{-1}$	$2.9 \times 10^{10}\gamma^{-1}$	$2.9 \times 10^{10}\gamma^{-1}$
T_{SSC}.....	$1.1 \times 10^{10}\gamma^{-1}$	$1.2 \times 10^{10}\gamma^{-1}$	$3.4 \times 10^{11}\gamma^{-1}$	$5.2 \times 10^{10}\gamma^{-1}$	$5.6 \times 10^{10}\gamma^{-1}$	$1.9 \times 10^{12}\gamma^{-1}$
T(1 GHz)	9.5×10^{6}	1.1×10^{7}	9.5×10^{7}	2.1×10^{7}	2.2×10^{7}	2.9×10^{8}
T(25 GHz)	1.9×10^{6}	2.2×10^{6}	1.9×10^{7}	4.1×10^{6}	4.4×10^{6}	5.8×10^{7}

NOTES.—Unless specified, all quantities are in cgs units, except for the radii which are in units of 10^{15} cm. The frequency ν_h is the high-frequency synchrotron cutoff. Time is given in 1979 Oct days. Radio quantities are given at 1 GHz and X-ray at 1 keV. The source had zero radius at $t_0 = 2.034$. The actual flux densities and optical depth were calculated from the observed quantities using a Doppler shift factor $D = 1/(1 + z) = 1.109$.

The quantities are n, electron distribution normalization; B, magnetic field; r, source radius; θ^R, jet opening angle in radians; $\theta°$, jet opening angle in degrees; S_x IC (SSC), X-ray spectral luminosity produced by the IC (SSC) process; $u_{B\,(e)}$, magnetic (electron) energy density; u_γ SSC (IC), synchrotron (external source) photon energy density; $\gamma(\nu)$, energy of electrons that radiate synchrotron photons of frequency ν; $T_{a\,(s)}$, adiabatic expansion (synchrotron radiation) loss time scale; $T_{IC\,(SSC)}$, Compton loss time scale due to external (synchrotron) photons; $T(\nu)$, minimum radiative loss time scale for electrons which radiate synchrotron photons at ν frequency.

observed flux, consistent with the assumption in this case that the X-ray emission is unrelated to the expanding source. The magnetic field in the equipartition model is much larger than the equipartition values $B \approx 0.01$ quoted in both Gilmore and Seaquist (1980) and Hjellming and Johnston (1981*a*) which were only lower limits based on a large source size upper limit (the source was unresolved).

The electrons which radiate 25 GHz synchrotron photons have the highest energy [labeled γ(25 GHz) in Table 4] of all the electrons necessary to produce observable emission, and consequently they have the shortest loss time scale due to either synchrotron or inverse Compton radiation. In all cases this loss time scale, T(25 GHz) in Table 4, is longer than adiabatic loss time scale, and any break in the electron distribution will not be manifest in the radio spectrum. In the IC and SSC models the source radius is of order 10^{13} cm, consistent with the shortest X-ray variation time scale of order 300 s (GB84). Since in the equipartition model the X-rays do not originate in the expanding source, the X-ray variability does not constrain the source size.

The width of the optical lines indicates an opening angle of ~ 0.04 rad or a half angle of 1°.8 (Margon 1984). The angular sizes of the IC and SSC models are well within this jet opening angle constraint. However, the source is a factor of 5 larger in the equipartition model, and the angular size is comparable to or slightly exceeds this constraint, indicating that the line-emitting region may occupy the core of the expanding source. If the thermal gas density n increases toward the center of the jet, then the optical line emissions should also increase toward the jet center since both clumping due to radiative cooling and the emissions from these clumps are proportional to n^2. In addition, since the pressure of nonrelativistic thermal gas, $P \propto n^{5/3}$, drops faster than that of relativistic electrons, $P \propto n^{4/3}$, the nonrelativistic gas may expand more slowly than the relativistic gas, and can be confined to the center of the jet.

Table 4 also includes the energy densities of the magnetic, electron, and photon fields. The particle energy density assumes that the electron distribution extends to $\gamma_{min} = 1$ and includes the electron rest mass [which constitutes a fraction $(p - 2)/(p - 1) = \frac{1}{6}$ for $\alpha = 0.6$ or $p = 2.2$ of the total energy]. SGJG explained the flattening of the X-ray spectrum by $\gamma_{min} > 1$, which reduces the energy density by the factor γ_{min}^{2-p} (which will still be of order unity for $\gamma_{min} \approx 100$).

In the IC or SSC models the electron energy density exceeds the magnetic energy density by 13 orders of magnitude, and the photon energy densities by eight! While equipartition may not be expected when the source is young and new electrons are continuously injected into the expanding source, the departure from equipartition is surprising, particularly if the injected electrons

are accelerated by processes involving the magnetic fields. We have seen that equipartition requires an X-ray origin outside the expanding source. In the following subsection we vary some of the modeling assumptions to determine whether the IC and SSC models can be brought closer to equipartition.

b) X-Rays from the Expanding Source

We have shown that the electron and magnetic fields are very far from equiparition in the models in which the observed nonthermal X-rays result from scattering within the expanding source entrained in the jets. Equipartition is favored because it results in the minimum energy configuration for a given observation, and indeed the energies in the equipartition model in Table 4 are far less than in the scattering models. While exact equipartition is perhaps not to be expected, and is occasionally found not to hold (for example in the radio-quiet AGN models in BG86), the differences between the energy densities in both the IC and SSC models for SS 433 are so large as to render these models suspect. Since observational uncertainties are incapable of bringing these models significantly closer to equipartition, major changes are required in the assumptions upon which the scattering models are based.

i) *Distance from Central Object*

Decreasing the distance of the expanding source from the central object R brings the source closer to equipartition for the IC model (the electron density drops because the photon density increases), but since the source remains approximately the same size, the jet opening angle will be absurdly large. Also if the source is traveling at $v = 0.26c$, as would be expected if it is entrained within the jet, then $R > 10^{15}$ cm at the second epoch for which a model is presented in Table 4, separated as it is from the first epoch by ~ 3 days.

ii) *Small Optical Depth to Synchrotron Self-Absorption*

As SGJG suggested, the radio turnover may result not from synchrotron self-absorption but from free-free absorption in the stellar wind surrounding the binary system. We see from equations (II.14)–(II.16) that as τ_s (the synchrotron optical depth) decreases, u_e/u_B decreases for the IC model (as is necessary for equipartition) and X-ray production by IC dominates SSC. However, this increases the size of the source as $\tau_s^{-1/2}$, and again the jet opening angle will be too large and the size will violate the X-ray variability constraint.

iii) *Synchrotron X-Ray Production*

The X-ray emissions could be direct synchrotron emission from the expanding sources, as SGJG suggested. Using the magnetic field from the equipartition model, $\gamma_{\max} > 3 \times 10^6$ is required to produce the observed X-ray flux. The synchrotron lifetime is about an order of magnitude shorter than the source crossing time, requiring reacceleration throughout the source. If the X-ray and radio fluxes are part of the same spectrum, a much tighter correlation could be expected. However, in only one of the two flares observed simultaneously by SGJG are the X-ray and radio fluxes correlated. Finally and most significantly, the synchrotron explanation for the X-ray flux does not explain why the spectrum flattens when the source flares, while inverse Compton scattering can very naturally produce this flattening with $\gamma_{\min} > 1$ (SGJG; BG86).

iv) *Clumped Emission*

As discussed in § II*c* above, clumping can only increase the ratio u_e/u_B, and thus cannot bring the source closer to equipartition.

v) *Small Pitch Angle and Anisotropic Magnetic Field*

The emission models are calculated under the assumption of a uniform pitch angle distribution. For small electron pitch angle ϕ the magnetic fields in Table 4 are essentially the effective magnetic field (i.e., $B_\perp$), while the actual magnetic field would be $B/\sin\phi$. Thus the magnetic energy density could be a factor of $1/\sin^2\phi$ larger. Since $u_e/u_B \approx 10^{13-14}$, $\sin\phi \approx 10^{-7}$. It is unlikely that such a small pitch angle would survive. If the magnetic field is tangled, then the electrons would soon find that the field has changed direction, and a small pitch angle would suddenly increase. If the field were aligned parallel to the jet, the electrons would travel down the jet at a velocity approaching the speed of light, not $0.26c$. However, the polarization observations (Hjellming and Johnston 1981*a*) show that the field is perpendicular to the jet, suggesting that the field is toroidal, at least on scales of $\sim 10^{16}$ cm, and the curvature of the field would change the pitch angle. In addition, electrons emit most of both the synchrotron and scattered photons along their direction of motion. Consequently, most of the radiation from electrons with small pitch angle to the magnetic field will be radiated along the magnetic field. Thus it is unlikely that a small pitch angle can be invoked to increase the magnetic field.

vi) *Alternative Source of X-Ray Emission*

We are left with the conclusion that the X-rays are not produced by scattering by the same nonthermal electrons within the expanding source. This is consistent with other observational factors. The two flares observed by SGJG demonstrate that the correlation between the radio and X-ray fluxes differs from flare to flare, even if ultimately they are triggered by the same mechanism (e.g., an accretion surge; GB84). In addition, the *COS B* upper limits in the 70–150 MeV band (Bignami 1981, private communication; see discussion below) indicate that the scattered spectrum must end below 70 MeV. This upper limit requires $\gamma_{\max} < 10^3$, while the 25 GHz radio observations require $\gamma_{\max} > 10^4$ with the magnetic fields in the scattering models, leading to a contradiction. Finally, as discussed in § IV, a single source within the binary system can explain all the X-ray observations from SS 433.

c) Expanding Source

Although we find that the X-ray flares do not originate in the same source as the radio emissions, the evolution of the radio flares nonetheless provides information about the expanding radio source. Of the two contemporaneous flares from SS 433 observed by SGJG, the first is more tractable to understanding than the second, and will be analyzed in detail here. The implications of the complexity of the second flare will be discussed below. Following SGJG, the radio observations of this first flare can be understood

TABLE 5

SS 433 RADIO FLARE

Date (Oct 1979 UT)	S_ν (Jy at 1 GHz)	t_s (at 1 GHz)
5.21	1.15 ± 0.07	6.25 ± 1.14
6.06	2.25 ± 0.16	5.20 ± 0.70
7.06	1.85 ± 0.08	2.55 ± 0.35
8.09	1.05 ± 0.06	0.70 ± 0.30
9.09	0.40 ± 0.05	0.00 ± 0.50

NOTES.—Fluxes and optical depths are fitted values from SGJG, and errors are our estimates based on propagating the errors on the observed values in SGJG. Spectral index of $\alpha = 0.6$ has been assumed, and a quiescent component of 1.23 Jy at 1 GHz was subtracted.

as the sum of quiescent emission and a sometimes self-absorbed flaring component. Table 5 presents the optically thin radio flux and synchrotron self-absorption optical depth found by SGJG after subtracting off the quiescent flux; we have propagated the errors from the flux measurements to provide errors on these quantities.

To analyze the evolution of the observable quantities, the expansion parameter $\chi = 1 + t/t_0$, equivalent to determining when the flare began, must be determined. As can be seen from equation (II.3), $\chi \propto (S_\nu/\tau_s)^{1/(d-e_1+m/2)}$, and thus a linear fit to $(S_\nu/\tau_s)^{1/(d-e_1+m/2)}$ determines $\chi(t)$ for a given model. The acceptability of the linear fit for different values of the indices d, e_1, and m (defined in Table 1) constrains the range of permitted models. Models with $2 \leq d \leq 3$ and $1 \leq m \leq 2$ are statistically acceptable due to the large errors, particularly on the last value of τ_s. Nonetheless, the fit to this last point is best for spherical expansion ($d = 3$). For spherical expansion ($d = 3$ and $m = 2$) we find by a weighted least-squares fit that the flare began at 2.034 ± 0.246 1979 October.

The increase and slow decrease of the optically thin synchrotron flux indicates that additional nonthermal electrons must be injected into the source. Thus the electron injection function $F(\chi)$ increases with χ. This function can be determined empirically from the evolution of the different observables for a given source model (the type of expansion is required to separate the power-law dependence on χ from $F(\chi)$; see eqs. [II.1], [II.2], [II.9], [II.10]). The similarity of the injection functions as derived independently from the synchrotron flux and optical depth provides a consistency check on the source model.

For the SS 433 flare we find that the different methods of calculating $F(\chi)$ are most consistent with each other for an $m = 2$ magnetic field dependence (i.e., $B \propto r^{-2}$), whether the expansion is two- or three-dimensional, although once again the differences between the different determinations of $F(\chi)$ are not so striking for $m < 2$ as to exclude any particular set of indices. Figure 2 presents $F(\chi)$ for different observables for a model with spherical expansion and $m = 2$. A large error in the small flaring radio flux at day 9.09 (particularly if the quiescent radio component was overestimated) may explain the decrease in $F(\chi)$ determined from the radio flux [$F(\chi)$ should never decrease].

Even though we argued in § III*b* above that the X-ray flux most likely does not originate as scattered emission from the expanding source, we include in Figure 2 the values of $F(\chi)$ calculated under the assumption that the X-ray emission was produced by either the IC or SSC processes in the expanding source. The sharp increase in the X-ray determined $F(\chi)$ curves at late times may be due to X-ray emission from the next flare which is still optically thick to radio waves but observable in the X-ray band.

Although the exact shape cannot be determined, the radio determined $F(\chi)$ curves in Figure 2 appears to be a straight line. If the relevant processes are injection and expansion (and therefore eq. [II.20] defines $F(\chi)$), then for spherical expansion and $\alpha = 0.6$ the injection rate must be a decreasing function of χ. If we assume the total injection rate (particles per time over the entire source) is proportional to $q \propto \chi^{-\xi}$ and $F(\chi)$ is close to a line, then $1 < \xi < 2$. Since the volume increases as χ^d, the injection rate per volume falls as $\chi^{-\xi-d}$, or for the spherical case as $\chi^{-4} - \chi^{-5}$. Note that SGJG's data extend up to 1 week after the source was ejected.

Spencer (1984) tracked radio knots from SS 433 for up to from ~30–100 days after ejection from the central source and found that the surface brightness (flux per beamwidth) decreased as $t^{-1.8}$. As he points out, this decrease is much slower than would be expected from spherical expansion without injection, even though the knots expand in the two observable dimensions. If we once again assume $q \propto \chi^{-\xi}$, then for spherical expansion (and $m = 2$) Spencer's observations require $\xi = -2.4$ if $\alpha = 0.6$ and $\xi = -3.2$ if $\alpha = 1$ (the spectral index indicated by Spencer's observations). On the other hand, if we require equipartition between the electron and magnetic fields, then $\xi = -\frac{4}{9}$ if $\alpha = 0.6$ and $\xi = -0.6$ if $\alpha = 1$. Thus the total injection rate *increases* with time for the latter times observed by Spencer as opposed to the decrease implied by the data of SGJG for earlier times. Note that injection proportional to the surface area of the expanding sphere gives $\xi = -2$. It appears that the nature of the injection changes as the knot moves away from the central source.

The large value of F after 3 days indicates that most of the electrons are freshly injected. Consequently the emissions from the source largely reflect the electron acceleration conditions at the time of emission. This may explain the different rates of electron injection observed by SGJG up to 1 week after the source was injected into the jets and by Spencer (1984) over a period 30 to 100 days after injection. This sensitivity to local conditions may also explain the complex behavior of the radio knots Schilizzi, Romney, and Spencer (1984) tracked.

IV. A CENTRAL NONTHERMAL X-RAY SOURCE IN SS 433

In § III we found that models of SS 433 where the observed X-rays are produced by scattering in the jets are far out of equipartition. An alternative model is a compact nonthermal source within the binary system which is self-absorbed at radio

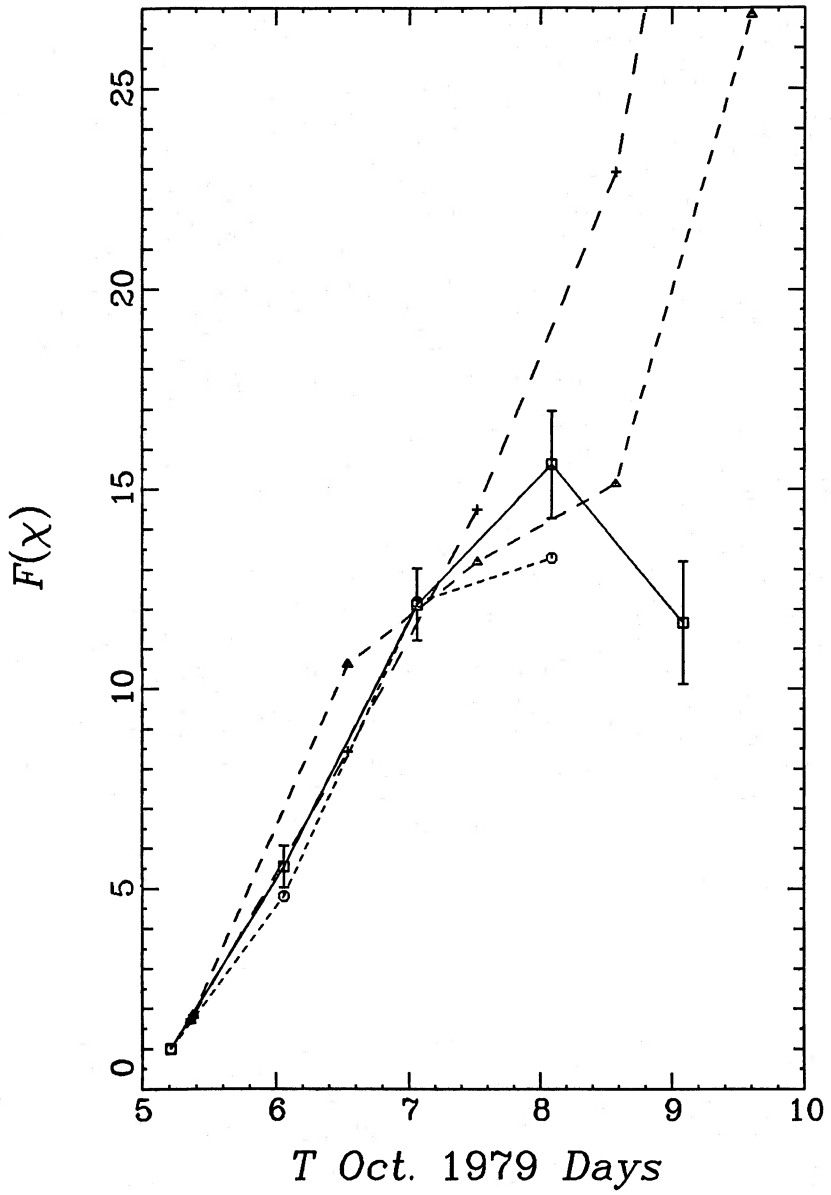

FIG. 2.—Injection function $F(\chi)$ as a function of time calculated from different observed quantities for a spherically expanding source with magnetic flux conservation ($B \propto \chi^{-2}$). Solid line is calculated from the radio flux; curve with the small dashes from the synchrotron optical depth τ_s; curve with the medium dashes from the X-ray flux, assuming it is produced by IC; and curve with the large dashes from SSC produced X-ray flux.

frequencies and masked by thermal emission in the infrared through ultraviolet bands, but which scatters thermal optical photons from both the accretion disk and companion star into the X-ray band. The resulting source morphology is similar to that of radio-quiet AGNs (BG86): radio emission from extended jets at various distances from the central engine, and X-ray emission by scattering of thermal photons in a compact nonthermal source surrounding the central engine.

Observations of X-ray eclipses, seen once each by the *Einstein* (GB84) and *EXOSAT* (Watson *et al.* 1986) telescopes, indicate that some fraction of the X-ray flux originates within the binary system. Since neither eclipse was observed to be total (the temporal resolution was insufficient to determine a minimum flux), nor did they occur during a flare, they do not prove conclusively that the flaring component is located within the binary. However, they do show that there is an X-ray source within the binary, and thus it is likely that all the (nonthermal) X-ray emission originates from one source within the binary.

Similarly, the fraction of the X-ray flux observed by *Einstein* that was thermal is unknown. The iron lines found by *EXOSAT* demonstrate that occasionally the source does radiate thermal X-rays. However, the absence of lines and the variation of the X-ray spectral index (GB84) indicate that the flux was predominantly nonthermal during the *Einstein* observations. As discussed in § I, the radio behavior differed between the *Einstein* and *EXOSAT* observations. Since we are interested in the magnitudes of the physical parameters of a central nonthermal source, and our models will not change significantly if some fraction of the X-ray flux density was thermal, we have assumed that it was entirely nonthermal.

If the nonthermal source is centered on the compact object, then most likely both the photon and electron distributions are both

nonspherical. Indeed the accretion disk surrounding the compact object radiates anisotropically (as shown by the 164 day variation of the optical light curve), and the jets are probably ejected along the axis of the accretion disk. The photon spectrum at a given point will be characteristic of the range of temperatures of the nearest region of the disk and thus the frequency distribution will vary spatially. Finally, only part of the thermal photons is produced by the accretion disk; about one-third is emitted by the stellar companion (Cherepashchuk 1981).

Despite all these complications, we will model the central source as a homogeneous sphere of relativistic electrons with a single temperature blackbody point source embedded at its center. The temperature of this thermal source is 4×10^4 K and its luminosity is 2.6×10^{39} ergs s^{-1}, consistent with the observations of Wagner (1983, 1986), as discussed in § III*a*. Given the uncertainties discussed above and the insensitivity of the scattered spectrum to the details of the soft photon spectrum, any attempt to use a more sophisticated soft photon spectrum will not increase the accuracy of the calculation.

In constructing models of this central compact source we require that: the synchrotron emission does not exceed the 90 GHz upper limit of 0.14 Jy (Landau, Epstein, and Rather 1980); the X-ray synchrotron spectrum does not exceed the X-ray observations; the scattered spectrum is consistent with the *COS B* limits on the 70–150 MeV flux (Bignami 1981, private communication); and the electron and magnetic field energy densities are in equipartition. Since the synchrotron spectrum is not observed due to either self-absorption or masking by thermal emission, there are not enough observations or constraints to define the model properly, and the additional physically reasonable assumption of equipartition is required. We assume that the spectral index is $\alpha = 0.6$, which appears to be the quiescent X-ray spectral index. The 10 keV spectral luminosity of 4.72×10^{-29} erg s^{-1} Hz^{-1}, calculated from the MPC observations for 1979 October 5.21, is chosen because $\gamma_{\min} > 1$ reduces the flux at lower energies.

While the observations do not prove conclusively that the flaring X-ray component is the same size as the eclipsed component (since only part of the X-ray source may flare or be eclipsed), it is likely that the two components are the same size, and thus the flaring component should be large enough so that it would not be eclipsed completely. Based on the binary model for SS 433 (see BG84) the X-ray source should be between 3×10^{11} and 10^{12} cm.

We therefore present four models in Table 6 constructed using a variant of the methodology in equations (II.13)–(II.16). For all these models there must be either a cutoff or a break in the synchrotron spectrum below the X-ray band so as not to exceed the observed X-ray fluxes. A maximum break energy ν_b calculated from the model's optically thin synchrotron flux and the observed X-ray flux is also presented in Table 6.

Finally the *COS B* upper limit of 2×10^{-6} photons cm^{-2} s^{-1} in the 70–150 MeV band (Bignami 1981, private communication) requires a cutoff in the scattered spectrum below 70 MeV. Since the bulk of the optical photons which are scattered are at 10^{15} Hz, the electron distribution must have a cutoff below $\gamma_{\max} < 3 \times 10^3$. By the same argument, to produce the continuum X-ray flux observed to ~ 10 keV, $\gamma_{\max} > 100$. Thus there is a wide range of permissible break frequencies: from $\nu_b = 4 \times 10^{11}$ Hz to 9×10^{14} Hz.

Figure 3 shows the resulting spectrum, observed and calculated, as it appeared on 1979 October 5.21. If possible, the observations are from the same day. The model includes the blackbody source in the binary system, a central nonthermal source (model 2 in Table 6), and the expanding equipartition source in the approaching jet (see Table 4). Synchrotron radio emission originates in the jets, while scattering by the central source produces the X-ray spectrum. The flattening of the scattered spectrum ($\alpha = 0.3$ as opposed to the 0.6 of the radio spectrum) results from $\gamma_{\min} > 1$, as discussed by SGJG and BG86. Note that as discussed the thermal spectrum used in the model is simpler than indicated by observation.

The Compton optical depth τ_C for the central source in Figure 3 is 6.6×10^{-6}. The electrons scatter only a small fraction of the optical photons that pass through the central source, and therefore do not modify the optical spectrum. The second-order scattered spectrum is far less bright than that produced by the first-order scattering, and will not violate the *COS B* limits. As a consequence of this small τ_C, the SSC spectrum is about three orders of magnitude fainter than the IC spectrum.

The light travel time across the source is less than the minimum variability time scale of 300 s (and even on this time scale the variations are small). It is not surprising that greater variability is not seen on shorter time scales because these models are large compared to the Schwarzschild radius of the putative 10 $M_\odot$ black hole ($\sim 10^6$ cm), and the characteristic velocities (derived from the gravitational potential) are small compared to the speed of light. Since electrons that scatter the thermal photons must have $\gamma \approx 10$–100, their lifetimes due to Compton losses (which is shorter than their synchrotron lifetimes) are comparable, if not less than the light crossing time. The actual electron crossing time will be even longer because the electrons will diffuse at velocities $v \sim v_A < c$. Thus the electrons are not created at the center of the source because they cannot escape the source within their Compton lifetime. Indeed, the shortest X-ray time scale of over 300 s may correspond to the time scale for energy to leak out of the

TABLE 6

MODELS OF CONTROL NONTHERMAL SS 433 SOURCE

Model	τ_s	S_r (Jy)	n	B	r	$t_{\rm cross}$	$t_{\rm IC}$	$S_{\rm SSC}$	$u_{\rm IC}/u_B$
1.....	6.1×10^6	7.	3.2×10^7	56.6	7.5×10^{11}	25	$325\gamma^{-1}$	9.3×10^{-33}	289
2.....	8.2×10^6	5.	4.2×10^7	65.1	5.7×10^{11}	19	$186\gamma^{-1}$	6.6×10^{-33}	383
3.....	1.1×10^7	3.5	5.7×10^7	75.7	4.2×10^{11}	14	$102\gamma^{-1}$	4.7×10^{-33}	515
4.....	1.5×10^7	2.5	7.5×10^7	86.9	3.2×10^{11}	11	$58.5\gamma^{-1}$	3.3×10^{-33}	682

NOTES.—Unless otherwise indicated, units are cgs. Radio quantities are given at 1 GHz and X-ray at 10 keV. The quantities are τ_s, synchrotron optical depth; S_r, radio flux density; n, electron distribution normalization; B, magnetic field; r, source radius; $t_{\rm cross}$, light travel time along radius; $t_{\rm IC}$, electron lifetime due to Compton losses; $S_{\rm SSC}$, X-ray flux density due to SSC process; $u_{\rm IC}/u_B$, ratio of photon to magnetic energy densities.

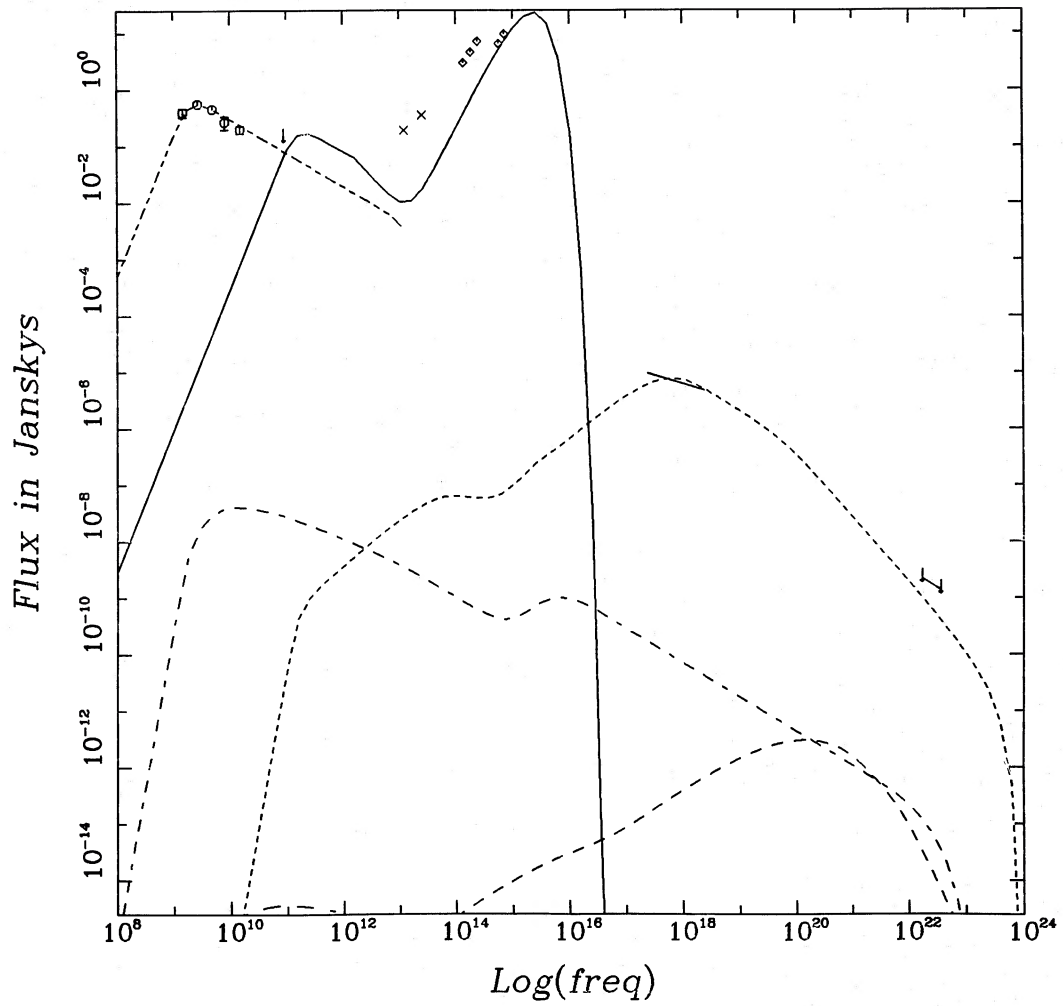

FIG. 3.—Model and observations of SS 433 on 1979 October 5.21. The model consists of a blackbody source in the center of the binary system ($L = 2.6 \times 10^{39}$ ergs s^{-1}, $T = 4 \times 10^4$ K) surrounded by a compact nonthermal source (*solid infrared through ultraviolet curve*) and expanding source in the approaching jet (*dash-dot-dot radio curve*) at a distance of 2.13×10^{15} cm from the central object. The once-scattered spectrum from the expanding source (*dot-dash curve*) is significantly below the scattered spectrum from the central source (*small dashed curve*), and is exceeded at high frequencies by the twice-scattered spectrum from the central source (*large dashes*). Radio observations are from SGJG, while 90 GHz upper limit is from Landau, Epstein, and Rather (1980). *IRAS* 12 and 25 μm observations were provided by Gillett (1985, private communication). The near-infrared and optical observations from Giles *et al.* (1980) were dereddened assuming $A_V \approx 7.5$. The *Einstein* 1–10 keV observations are from GB84, and the *COS B* 70–150 MeV upper limits were provided by Bignami (1981, private communication). The radio, infrared, optical, and X-ray observations are all from 1979 5 October. Parameters of the central source are $B = 65.1$ G, $r = 5.66 \times 10^{11}$ cm, $dn = 4.21 \times 10^7 \gamma^{-2.2} d\gamma$ cm^{-3} for $10 \leq \gamma \leq 100$, and $dn = 4.21 \times 10^9 \gamma^{-3.2} d\gamma$ cm^{-3} for $100 \leq \gamma \leq 10^4$. Parameters of the expanding source are $dn = 4.72 \times 10^3 \gamma^{-2.2} d\gamma$ cm^{-3} for $1 \leq \gamma \leq 2600$, $B = 0.697$ G, and $r = 7.10 \times 10^{13}$ cm. Emissions from the expanding jet source are blueshifted by the relativistic factor $D = 1/(1 + z) = 1.109$.

source. Consequently, the electrons must be reaccelerated within the source, with the break energy reflecting the distance between reacceleration centers, as discussed in BG86 for radio-quiet AGNs. The average photon energy density (due predominantly to thermal photons) in these sources is over a factor of 100 larger than the magnetic and electron energy densities. This unidirectional photon flux may induce plasma instabilities and strong shocks throughout the source which reaccelerates the electrons.

The resulting X-ray model of SS 433 is strikingly similar to the radio-quiet AGN model presented in BG86. In that model, a compact nonthermal source in the AGN core is synchrotron self-absorbed at radio frequencies, and the observed radio emissions originate in the jets outside the core. In the central nonthermal source the electrons both radiate and are reaccelerated throughout the source resulting in a "broken" electron distribution. The resulting synchrotron spectrum will also consist of two power laws with a break typically in the infrared. The flatter low-energy end of the electron distribution scatters predominantly thermal photons from the ultraviolet into the X-ray band, and the spectral index of the resulting scattered spectrum reflects the distribution of low-energy electrons. The energy density of this thermal ultraviolet spectrum is comparable to or greater than the magnetic field energy density, and thus Compton cooling of the electrons dominates.

While equipartition was assumed in constructing the models of the SS 433 due to the paucity of observational information, the magnetic field can dominate the electron energy density as in the AGN models. For example, if in SS 433 the magnetic field energy density were 10 times greater than the electron energy density, then in comparison with the equipartition models the electron density would be a factor of 0.29 smaller, the magnetic field a factor of 1.7 larger, and the source radius only a factor of 1.14 larger.

V. SUMMARY

We have extended the standard expanding source model of van der Laan (1966) to make it applicable to a broader range of physical circumstances. The two major refinements of the model are the incorporation of the X-ray emissions from these sources and the continuous injection of electrons as the source expands. We also allow for one- or two-dimensional expansion in addition to the standard spherical expansion. We consider three aspects of the model: (1) the evolution of the observables; (2) the determination of the physical parameters at a given time from the observables; and (3) the physics applicable to the source (such as the type of electron distribution and the likely expansion indices). The addition of X-ray emission to the expanding source model and the importance of tracking the size of the source and its distance from the central object (e.g., the AGN core or the binary in SS 433) demonstrate the importance of future simultaneous X-ray and radio observations, particularly by the next generation of instruments, *AXAF* and the *VLBA*.

We applied the expanding source methodology to the simultaneous radio and X-ray observations of SS 433 reported by Seaquist *et al.* (1982) and Grindlay *et al.* (1984) that trace two flares. Both inverse Compton scattering of optical photons and synchrotron–self-Compton scattering produce comparable X-ray fluxes if the X-rays originate in the expanding sources entrained in the jets. Although these radiation models are otherwise consistent with the binary and jet models of the SS 433 system, the electron energy density exceeds the magnetic field energy density by 13 orders of magnitude. If equipartition is required, then the X-ray flux drops by five orders of magnitude, and the X-rays must be emitted by another source.

The evolution of the radio source requires continuous electron injection, although the time dependence of this injection in the few days after the expanding source was ejected from the binary is different from the time dependence evident from the observations of Spencer (1984) weeks after ejection. The observations are insufficient to distinguish between different types of expansion, although they are consistent with spherical expansion of a "plasmon" moving out in the jet, with the magnetic field decreasing as $B \propto r^{-2}$.

An X-ray source within the binary system is suggested by the X-ray eclipse observations (although at times this X-ray producing component may be in part thermal; see discussion in § I). It is possible to construct a compact nonthermal source surrounding the optical photon source (most likely the accretion disk, although the companion's luminosity is about half that of the disk; Cherepashchuk 1981) which is optically thick (and thus unobservable) at radio frequencies and which scatters optical photons into the X-ray band. The resulting source morphology is similar to the AGN model of Band and Grindlay (1986): the observed radio emissions originate in the jets, while the X-rays are produced in a radio-quiet core. This similarity strengthens the identification of SS 433 as a galactic model of an AGN.

We thank Larry Molnar for discussions on expanding sources and on data reduction techniques, and for a critical reading of the manuscript. We thank Fred Gillett for preliminary flux densities from *IRAS* pointed observations of SS 433 and Ralph Fiedler for the radio behavior during the *EXOSAT* observations from the Green Bank interferometer monitoring program. This work was supported in part by NASA grant NAS8-30751.

REFERENCES

Band, D. L. 1987, in preparation.
Band, D. L., and Grindlay, J. E. 1984, *Ap. J.*, **285**, 702 (BG84).
———. 1985, *Ap. J.*, **298**, 128 (BG85).
———. 1986, *Ap. J.*, **308**, 329 (BG86).
Catchpole, R. M., Glass, I. S., Carter, B. S., and Roberts, G. 1981, *Nature*, **291**, 392.
Cherepashchuk, A. M. 1981, *M.N.R.A.S.*, **194**, 761.
Giles, A. B., King, A. R., Cooke, B. A., McHardy, I. M., and Lawrence, A. 1979, *Nature*, **281**, 282.
Giles, A. G., *et al.* 1980, *Nature*, **286**, 689.
Gilmore, W., and Seaquist, E. R. 1980, *A.J.*, **85**, 1486.
Grindlay, J. E., Band, D. L., Seward, F., Leahey, D., Weisskopf, M. C., and Marshall, F. E. 1984, *Ap. J.*, **277**, 286 (GB84).
Hjellming, R. M., and Johnston, K. J. 1981*a*, *Nature*, **290**, 100.
———. 1981*b*, *Ap. J. (Letters)*, **246**, L141.
Jones, T., O'Dell, S., and Stein, W. 1974, *Ap. J.*, **188**, 353.
Johnston, K. J., *et al.* 1981, *A.J.*, **86**, 1377.
———. 1984, *A.J.*, **89**, 509.
———. 1985, *Bull. AAS*, **16**, 914.
Kardashev, N. S. 1962, *Soviet Astr.—AJ*, **6**, 317.
Königl, A. 1981, *Ap. J.*, **243**, 700.
Landau, R., Epstein, E. E., and Rather, J. D. G. 1980, *A.J.*, **85**, 363.
Margon, B. 1984, *Ann. Rev. Astr. Ap.*, **22**, 507.
Marscher, A. P., and Brown, R. L. 1975, *Ap. J.*, **200**, 719.
Molnar, L. A. 1985, Ph.D. thesis, Harvard University.
Molnar, L. A., Reid, M. J., and Grindlay, J. E. 1984, *Nature*, **310**, 662.
———. 1985, in *Radio Stars*, ed. R. M. Hjellming (Dordrecht: Reidel), p. 329.
Murdin, P., Clark, D., and Martin, p. 1980, *M.N.R.A.S.*, **193**, 135.
Niell, A. E., Lockhart, T. G., and Preston, R. A. 1981, *Ap. J.*, **250**, 248.
Peterson, F. W., and Dent, W. A. 1977, *Ap. J.*, **186**, 421.
Rybicki, G. B., and Lightman, A. P. 1979, *Radiative Processes in Astrophysics* (New York: Wiley).
Schilizzi, R. T., Miley, G. K., Romney, J. D., and Spencer, R. E. 1981, *Nature*, **290**, 318.
Schilizzi, R. T., Romney, J. D., and Spencer, R. E. 1984, in *IAU Symposium 110, VLBI and Compact Radio Sources*, ed. R. Fanti, K. Kellerman, and G. Setti (Dordrecht: Reidel), p. 1.
Seaquist, E. R., Garrison, R. F., Gregory, P. C., Taylor, A. R., and Crane, P. C. 1979, *A.J.*, **84**, 1037.
Seaquist, E. R., Gilmore, W. S., Johnston, K. J., and Grindlay, J. E. 1982, *Ap. J.*, **260**, 220 (SGJG).
Seaquist, E. R., Gilmore, W., Nelson, G. J., Payten, W. J., and Slee, O. B. 1980, *Ap. J. (Letters)*, **241**, L77.
Spencer, R. E. 1979, *Nature*, **282**, 483.
———. 1984, *M.N.R.A.S.*, **209**, 869.
Tucker, W. H. 1975, *Radiation Process in Astrophysics* (Cambridge: MIT Press).
Unwin, S. C., *et al.* 1985, *Ap. J.*, **289**, 109.
van der Laan, H. 1966, *Nature*, **211**, 1131.
Vitello, P., and Pacini, F. 1977, *Ap. J.*, **215**, 452.
Vitello, P., and Salvati, M. 1976, *Phys. Fluids*, **19**, 1523.
Wagner, R. M. 1983, *Bull. AAS*, **14**, 880.
———. 1986, *Ap. J.*, **308**, 152.
Walker, R. C., *et al.* 1981, *Ap. J.*, **243**, 589.
Watson, M., Stewart, G., Brinkman, W., and King, A. 1986, *M.N.R.A.S.*, in press.
Wynn-Williams, C. G., and Becklin, E. E. 1979, *Nature*, **282**, 810.

D. L. BAND: L-413, IGPP–Lawrence Livermore National Laboratory, Box 808, Livermore, CA 94550

J. E. GRINDLAY: Harvard-Smithsonian Center for Astrophysics, 60 Garden Street, Cambridge, MA 02138